Fast in-Band Position-Aided Beam Selection in Millimeter-Wave MIMO

(article starts on next page)

Fast in-Band Position-Aided Beam Selection in Millimeter-Wave MIMO

GABRIEL E. GARCIA [ID][1], **NIL GARCIA**[1], **(Member, IEEE),**
GONZALO SECO-GRANADOS [ID][2], **(Senior Member, IEEE),**
ELEFTHERIOS KARIPIDIS[3], **(Member, IEEE),**
AND HENK WYMEERSCH [ID][1], **(Member, IEEE)**

[1]Department of Electrical Engineering, Chalmers University of Technology, 41296 Gothenburg, Sweden
[2]Department of Telecommunications and Systems Engineering, Universitat Autònoma de Barcelona, 08193 Barcelona, Spain
[3]Ericsson Research, 16440 Stockholm, Sweden

Corresponding author: Gabriel E. Garcia (ggarcia@chalmers.se)

ABSTRACT Millimeter-wave (mm-wave) and massive multiple-input-multiple-output technologies appear as key enablers in future emerging wireless communication systems. Propagation in mm-wave communications is well described by geometric channel models, where a clear relation between communication and positioning arises. On one hand, initial access, a procedure that precedes high data rate transmission and consists of beam selection and alignment between two devices, can benefit from position information. On the other hand, accurate positioning relies on high-quality communication links with proper beam alignment. This work analyzes the interplay between communication and positioning, proposes a new in-band position-aided beam selection protocol considering scenarios with line-of-sight and reflected paths, and possible beam alignment errors. Simulation results show significant reductions in latency with respect to standard beam selection protocols.

INDEX TERMS Cramer-Rao bounds, initial access, millimeter wave communication, MIMO, orientation, positioning, position measurement, protocols.

I. INTRODUCTION

Emerging wireless communication systems are intended to address stringent requirements in terms of (i) throughput (1 Gb/s or higher), (ii) low latency (less than one 1 ms), (iii) ultra reliability, and (iv) higher connectivity [1]–[5]. Millimeter-wave (mm-wave) communications have recently gained attention in cellular systems operating at frequencies between 30 to 300 GHz, and where the available bandwidths are wider than in current cellular networks. Moreover, they have been presented as a key enabler to achieve the future communication system's requirements along with its integration with multiple-input-multiple-output (MIMO), using a large number of antennas. This integration facilitates the exploitation of spatial multiplexing and provides high data rates to users within a wide range of applications, from

The associate editor coordinating the review of this manuscript and approving it for publication was Wei Xu [ID].

wearables [6] to automotive [7]. However, operating in those bands comes at cost in terms of the high isotropic propagation loss. Hence, solutions involving highly directional antennas to improve link budgets as well as the implementation of beamforming (BF) both at the transmitter and the receiver have been proposed [8]–[10]. These solutions rely on the knowledge and characterization of the mm-wave MIMO propagation channel.

The mm-wave channel can be characterized with few parameters by means of stochastic geometrical channel models (SGCM), which have become an attractive approach, given the propagation behavior of mm-wave where the line-of-sight (LOS) and a few dominant multipath components contribute to the received power [11]–[15]. SCGMs relate the propagation to the geometry of the operating scenario, thus creating an interplay between the communication channel and the positions of the transmitter and receiver, as well as the environment [11]–[15]. On one hand, the positions

of devices can be estimated through the exchange of mm-wave signals, which in turn requires the establishment of a communication link [16], [17]. On the other hand, the establishment of a communication link can be performed by a dedicated protocol that searches within the angle space: angle of departure (AOD) [18], and angle-of-arrival (AOA) [19], which in turn are geometrically related to the positions of the devices. Hence, the positioning and communication aspects are inherently intertwined [20]. This synergy suggest devoting efforts towards finding a joint solution where both the communication and the positioning aspects can benefit from each other and result in an overall better system performance. This synergy is especially pronounced in the initial access problem [4], where position information can reduce the time to set up a communication link and where the exchange of radio signals provides position information.

Initial access has the aim of establishing a sufficient link budget, discovering suitable propagation paths for transmission, and discarding paths with low gain [4], [21], [22]. Beam selection protocols are designed to tackle the initial access problem. These protocols may or may not exploit context or structure information such as position or channel sparsity. Conventional protocols such as exhaustive beam selection schemes, or received signal power protocols do not consider the positioning information in an explicit manner [8]. A great deal of research has been devoted to reduce the time for initial access, including methods for different array types (analog [8], [23], hybrid [14], arrays of subarrays [24], [25]), as well as methods that adapt rate and power [26], [27], operate in tracking mode [28]–[30], rely on low-complexity non-coherent processing [31], or consider learning-based approaches [32].

Alternatively, context-based methods can exploit position information. Position information can be harnessed from *out-of-band* technologies, (e.g., Global Positioning System, displacement sensors) in contrast to possible *in-band* solutions, where location information is obtained from the mm-wave communication signal itself. Contributions such as [33]–[36] exploit position information obtained from out-of-band technologies. For instance, in [34], a position-aided beam alignment solution is proposed with the use of position information obtained from the on-board train system. A database-based solution is proposed in [35], where channel propagation information is linked to the user's geographical position. In [36], high-sensitivity displacement sensors provide information about the fixed-position networks nodes to perform beam alignment in mm-wave backhaul systems. In [33], location information is harnessed for fast channel estimation in a vehicular context. As out of band position information may not always be available, in-band position information is a promising alternative or complement.

In this paper, we extend our work from [37] and propose a fast in-band position-aided beam selection protocol with the goal of (i) reducing the set-up time of the initial access problem; (ii) determine the location and orientation of a device. The main difference of the current work with respect
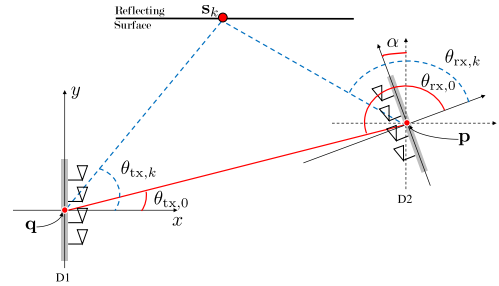

FIGURE 1. Two-dimensional MIMO system model with a D1 with known position and orientation, and a D2 with unknown position (p) and orientation (α), with reflective surface.

to [37] is the inclusion of both precoding and combining with hybrid arrays at both end of the link ([37] only considered precoding and digital receiver arrays), as well as an analysis of the positioning/SNR trade-off. In an a priori unknown environment with unknown device location, we propose to progressively refine knowledge regarding the device position and orientation during the initial access process, which allows us to quickly point fine beams towards the device. The method is evaluated using metrics relevant to communication (SNR and set-up time) as well as positioning (position error bound and orientation error bound). Our contributions are:

- A novel in-band positioning-aided beam selection protocol with the aim of reducing the set-up time of the initial access procedure for communication under beam alignment errors in the presence of a line-of-sight path and reflectors. The protocol is compatible with standard initial access procedures from the literature, but leads to faster link establishment.
- A numerical trade-off analysis between the final link SNR and the position error bounds, providing indications for future generation wireless communication systems, where adaptive initial access solutions can be implemented based on a specific performance metric.

The remainder of the paper is structured as follows. Section II presents the communication model. In section III, the conventional signal received power-based protocol description and its specifics are described. Then, in section V the joint positioning and beam selection protocol, its operation and specifications are introduced. Finally, numerical results are given in section VII, followed by the conclusions in section VIII.

II. SYSTEM MODEL

We consider a MIMO mm-wave system, consisting of a (reference) device D1 and a second device D2, equipped with analog arrays (single radio frequency chain per array) of N_t and N_r antennas, respectively. Both devices are assumed to lie on a plane with unobstructed line-of-sight. We denote the locations of D1 and D2 by $\mathbf{q} = [q_x, q_y]^T \in \mathbb{R}^2$ and $\mathbf{p} = [p_x, p_y]^T \in \mathbb{R}^2$, respectively,[1] and let $\alpha \in [0, 2\pi)$ be the

---

[1]The analysis can be extended to a 3-dimensional scenario with 2-dimensional antenna arrays. A 2-dimensional model and linear antenna arrays are assumed for simplicity.

Notation	Meaning
N_r	number of receive antennas
N_t	number of transmit antennas
$N_r'^{(i)} \leq N_r$	number of active receive antennas at iteration i
$N_t'^{(i)} \leq N_t$	number of active transmit antennas at iteration i
$M_r^{(i)}$	number of receive beams at iteration i
$M_t^{(i)}$	number of transmit beams at iteration i
N_s	number of subcarriers
N^i	number of OFDM symbols at iteration i
$\xi \in [0, 1]$	LOS energy
$\varepsilon \in [0, 1]$	required alignment error probability

angle of rotation of the D2 antenna array with respect to the coordinate system of D1 as shown in Figure 1. We assume that $\mathbf{q}$ is known and the rotation of D1 with respect to the absolute coordinate frame is set to zero, while $\mathbf{p}$ and α are unknown. The system model setup is general, however, it is compatible with downlink transmission since the location of the transmitter D1 (a base station) is generally known. A list of notations is found in Table 1.

A. GEOMETRIC CHANNEL MODEL WITH LOS AND REFLECTORS

For the LOS path, we can introduce the angle of departure (AOD) $\theta_{\text{tx},0}$ and angle of arrival (AOA) $\theta_{\text{rx},0}$, which are defined with respect to the absolute coordinate frame and to D2's local coordinate frame, respectively. We denote the LOS propagation delay as $\tau_0 = \|\mathbf{q} - \mathbf{p}\| / c$, where c is the speed of light. The environment can include non-line-of-sight (NLOS) paths. For each NLOS path, we assume the existence of an incidence point with location $\mathbf{s}_k$, $k \geq 1$, and the corresponding parameters are: the delay $\tau_k = \|\mathbf{q} - \mathbf{s}_k\| / c + \|\mathbf{s}_k - \mathbf{p}\| / c$, the AOD $\theta_{\text{tx},k}$, and the AOA $\theta_{\text{rx},k}$. The relation between the AOD and AOA of each path, and the locations $\mathbf{s}_k, \mathbf{p}$, and rotation α can be graphically observed in Figure 1. This relation is also valid when the NLOS path corresponds to a cluster of unresolved rays, and thus captures both specular and mixed specular/diffuse NLOS.

The transmitting device, D1, transmits OFDM signals at a carrier frequency f_c (or equivalently wavelength $\lambda = c/f_c$) and with bandwidth $B = 1/T_s$ over N_s subcarriers. The $N_r \times N_t$ channel matrix for subcarrier $n = 0, \dots, N_s - 1$ is given by [38]

$$\mathbf{H}[n] = \sqrt{N_t N_r} \sum_{k=0}^{K-1} h_k \, \mathbf{a}_{\text{rx}}(\theta_{\text{rx},k}) \mathbf{a}_{\text{tx}}^{\text{H}}(\theta_{\text{tx},k}) e^{-j2\pi \tau_k n / N_s T_s} \quad (1)$$

where h_k is a complex channel gain, and $\mathbf{a}_{\text{tx}}(\theta_{\text{tx},k}) \in \mathbb{C}^{N_t}$, $\mathbf{a}_{\text{rx}}(\theta_{\text{rx},k}) \in \mathbb{C}^{N_r}$ are the normalized antenna steering and response vectors, all associated with the k-th path. We assume uniform linear arrays (ULAs) in both D1 and D2, so that the steering and response vectors are computed as

$$[\mathbf{a}_{\text{tx}}(\theta_{\text{tx}})]_{l=0}^{N_t-1} = \frac{1}{\sqrt{N_t}} \exp\left(j \frac{2\pi l d}{\lambda} \sin \theta_{\text{tx}}\right) \quad (2)$$

$$[\mathbf{a}_{\text{rx}}(\theta_{\text{rx}})]_{l=0}^{N_r-1} = \frac{1}{\sqrt{N_r}} \exp\left(j \frac{2\pi l d}{\lambda} \sin \theta_{\text{rx}}\right), \quad (3)$$

where d is the antenna spacing.

B. TRANSMITTER

We assume the use of beamforming, implemented using phase shifters, and combined with antenna selection. Each transmission consists of N sequentially transmitted symbols $\mathbf{x}[n] = [x_1(n), \dots, x_N(n)]^{\text{T}}$ for each subcarrier $n = 0, \dots, N_s - 1$, with constant energy $E_x = \mathbb{E}[|x_k|^2]$. Hence, the transmitted signal model over subcarrier n can be expressed as $\mathbf{f}_m \mathbf{x}^{\text{T}}[n] \in \mathbb{C}^{N_t \times N}$ where $\mathbf{f}_m \in \mathbb{C}^{N_t \times 1}$ corresponds to a unit energy precoding vector for the $m \in \{1, \dots, M_t\}$-th beam. The precoding vector is expressed as

$$\mathbf{f}_m = \frac{1}{\sqrt{N_t'}} \left[e^{j\phi_{m,0}} \dots e^{j\phi_{m,N_t'-1}} \, \mathbf{0}_{N_t - N_t'} \right]^{\text{T}}, \quad (4)$$

where $\mathbf{0}_{N_t - N_t'}$ is defined as a null vector of size $N_t - N_t'$ and and $N_t' \leq N_t$ indicates the number of *active antennas*, which is used to control the beam width at the expense of the beam gain [39]. The values of $\phi_{m,i}$ are dependent on the specific codebook $\mathcal{C}_{\text{tx}}$ design for the transmitter, and can include [8]

- 2-bit phase shifters: The phases are constraint to $\phi_{m,i} \in \{0, \pi/2, \pi, -\pi/2\}$.
- Unconstrained directional: The phases are linearly increasing, $\phi_{m,i} = i\phi_{m,0}$, where $\phi_{m,0}$ is a spatial frequency, corresponding to a direction $\theta = \arcsin(\phi/(2\pi d/\lambda))$.

In the current paper, only 2-bit phase shifters are used for all protocols. These beams allow for a varying degree of controlled directionality. Fewer active antennas means larger array aperture and consequently broader beams.

C. RECEIVER

We denote the combining vector at the receiver for the $l \in \{1, \dots, M_r\}$-th beam as $\mathbf{w}_l \in \mathbb{C}^{N_r}$, and it can be expressed similarly to the precoding vector as in (4) where the number of active antennas at the receiver is $N_r' \leq N_r$. Then, the received signal vector for subcarrier $n = 0, \dots, N_s - 1$ for all N transmitted symbols under a given pair of precoding and combining vectors $(\mathbf{f}_m, \mathbf{w}_l)$, is expressed as a row vector of length N

$$\mathbf{y}_{l,m}^{\text{T}}[n] = \mathbf{w}_l^{\text{H}} \mathbf{H}[n] \mathbf{f}_m \mathbf{x}^{\text{T}}[n] + \mathbf{v}_l^{\text{T}}[n], \quad (5)$$

where $\mathbf{v}_l[n]^{\text{T}} \in \mathcal{CN}(0, \mathbf{I}_N N_0)$ denotes additive noise which is independent across subcarriers. Finally, we assume a feedback channel exists from D2 to D1 [40].

III. CONVENTIONAL BEAM SELECTION

The goal of a beam selection protocol is to minimize the beamforming set-up time within the initial access procedure. The IEEE 802.15.3c standard [41], which aims to realize Gb/s communication in wireless personal area network systems, includes an optional functionality based on the hierarchical codebooks described in [8]. This iterative protocol

relies on a multilevel beam tree search starting from lower resolution beams that cover large angular range per beam, moving towards higher resolution beams covering a smaller angular range based on the reference signal received power. We will describe a general beam selection protocol for D1 and D2 based on reference signal received power during the initial access procedure. It is important to note that the beam selection protocol does not exploit any position information.

A. GENERIC PROCEDURE

Under the conventional beam selection, the D1–D2 pair applies an iterative procedure, where at iteration i, a number of active antennas $(N_t^{'(i)}, N_r^{'(i)})$ is selected, as well as a set of $M_t^{(i)}$ transmitting beams $\mathcal{F}^{(i)} = \{\mathbf{f}_1^{(i)}, \ldots, \mathbf{f}_{M_t^{(i)}}^{(i)}\}$ and $M_r^{(i)}$ receiving beams $\mathcal{W}^{(i)} = \{\mathbf{w}_1^{(i)}, \ldots, \mathbf{w}_{M_r^{(i)}}^{(i)}\}$ from codebooks $\mathcal{C}_{\text{tx}}^{(i)}(N_t^{'(i)})$ and $\mathcal{C}_{\text{rx}}^{(i)}(N_t^{'(i)})$, which are a function of the contiguous active antennas [8]. Hence, we have $\mathbf{f}_m^{(i)} \in \mathcal{C}_{\text{tx}}^{(i)}(N_t^{'(i)})$ and $\mathbf{w}_l^{(i)} \in \mathcal{C}_{\text{rx}}^{(i)}(N_r^{'(i)})$, for $m = 1, \ldots, M_t^{(i)}$, and $l = 1, \ldots, M_r^{(i)}$, respectively. Beam overlapping occurs among beams that point towards the same direction and belong to distinct iteration codebooks with different number of active antennas and set of transmitting/receiving beams. For each of the $M_t^{(i)} \times M_r^{(i)}$ pairs $(\mathbf{f}_m, \mathbf{w}_l)$, a training OFDM signal is sent over N_s subcarriers, leading to an observation $\mathbf{y}_{l,m}^{\text{T}(i)}[n]$, and the corresponding received power is computed.

In particular, the receiver D2 first computes the received power for each beam pair and then determines the beams giving rise to the maximum energy

$$[\hat{l}, \hat{m}] = \arg \max_{(l,m)} \sum_{n=0}^{N_s-1} \left\| \mathbf{y}_{l,m}^{\text{T}(i)}[n] \right\|^2,$$

and sends back the value of $\hat{m}$ to D1 over the feedback channel. Second, both D1 and D2 determine the number of active antennas as well as a set of beams, for the next iteration $i + 1$, where $N_t^{'(i+1)} \geq N_t^{'(i)}$ and $N_r^{'(i+1)} \geq N_r^{'(i)}$, translating into more (or at least not less) directive beams at each iteration step. Note that D2 does not need to know which beams D1 transmits, provided the number of beams $M_t^{(i)}$ and $M_r^{(i)}$ are agreed upon beforehand.

To ensure that the protocol achieves a certain probability of correct alignment, one can increase the aggregated received energy by adapting the power per iteration [14], or by increasing the number of symbols N. We have chosen to adapt N at each iteration i and for any combination of transmit N_t' and receive antennas N_r', in such a way that the probability of misalignment at a given target distance and at each stage

$$\Pr\left([\hat{l}, \hat{m}] \neq \arg \max_{(l,m)} \nu_{l,m}\right),$$

is sufficiently small, where

$$\nu_{l,m} = \frac{E_x}{N_s} \sum_{n=0}^{N_s-1} |\mathbf{w}_l^H \mathbf{H}[n] \mathbf{f}_m|^2, \quad (6)$$

which is maximized under optimal alignment.

B. SELECTION OF THE NUMBER OF OFDM SYMBOLS

Given a target total error probability $P_{\text{err}} \ll 1$ and I number of iterations, we easily find the alignment error probability ε at each iteration i from the relation

$$P_{\text{err}} = 1 - (1 - \varepsilon)^I. \quad (7)$$

Note that this relation is not unique and many combinations of ε_i at iteration i could lead to the same P_{err}. We have chosen to use a fixed ε for each iteration. Given $\varepsilon = 1 - \exp(\log(1 - P_{\text{err}})/I)$, we find that (see Appendix A)

$$NN_s \approx \begin{cases} (Q^{-1}(\frac{\varepsilon}{2}))^2 \dfrac{2(2 + \nu_{l*-1,m*} + \nu_{l*,m*})}{(\nu_{l*,m*} - \nu_{l*-1,m*})^2} & N_t' > N_r' \\[2ex] (Q^{-1}(\frac{\varepsilon}{2}))^2 \dfrac{2(2 + \nu_{l*,m*-1} + \nu_{l*,m*})}{(\nu_{l*,m*} - \nu_{l*,m*-1})^2} & N_t' < N_r' \\[2ex] (Q^{-1}(\frac{\varepsilon}{4}))^2 \dfrac{2(2 + \nu_{l*-1,m*} + \nu_{l*,m*})}{(\nu_{l*,m*} - \nu_{l*-1,m*})^2} & N_t' = N_r' \end{cases}$$
$$(8)$$

where $Q(\cdot)$ is the Q function. From (8), we can immediately find $N^{(i)}$ for a specific iteration i. Note that for different iteration numbers, the values of N_t', N_r' as well as $\nu_{l,m}$ will vary, so that $N^{(i)}$ will generally decrease with the iteration index. Note also that under fixed number of subcarriers N_s, and directivity as a function of N_t' and N_r', the number of symbols $N(N_t', N_r', \varepsilon)$ serves as a tuneable design parameter which can be calculated for a specific required ε, or total error probability P_{err}. Observe that this calculation involves a given nominal channel $\mathbf{H}[n]$, from which $\nu_{l,m}$ are immediately derived.

C. PROTOCOL SPECIFICS

The above beam selection procedure can be instantiated in a number of ways, for example:

- *Exhaustive:* D1 and D2 can both use all available antennas and all possible associated beams (for orthogonal codebooks this number would be the same as the number of antennas) for only a single iteration. In that case, for $M_t = N_t$ and $M_r = N_r$, the total number of beam pairs scales as $\mathcal{O}(M_t M_r) = \mathcal{O}(N_t N_r)$ [4].
- *Hierarchical:* D1 and D2 can double the number of active antennas at each iteration, progressively increasing the beam directivity, while maintaining fixed values for M_t and M_r across all iterations. The total number of beam pairs scales as $\mathcal{O}(M_t M_r \max\left(\log_2 N_t, \log_2 N_r\right))$. Note that considering the codebook designs described in section II-B, a beam pointing towards a predefined direction from codebook $\mathcal{C}_{\text{tx}}^{(i)}(N_t')$ can be covered by 3 beams from codebook $\mathcal{C}_{\text{tx}}^{(i+1)}(2N_t')$ using double number of antennas pointing towards the same direction [37]. Hence, $M_t = M_r = 3$ is a reasonable value for all iterations.

We note that while the first approach requires a large number of D1/D2 beam pair transmissions, it has the advantage of evaluating the received energy $\sum_{n=0}^{N_s-1} ||\mathbf{y}_{l,m}^{\text{T}(i)}[n]||^2$ for the best possible beam pair. In contrast, the second approach performs

a fast depth-first search, but any mistake in early iterations leads to an inevitable loss in SNR.

IV. MM-WAVE POSITIONING DURING BEAM SELECTION

In this section, we analyze the tight relation between positioning information and beam alignment. First, we introduce our observation model based on the received waveforms. Then, we characterize the achievable positioning performance based on our observation model along with position estimation approaches.

A. OBSERVATION MODEL

The signals as observed in (5), depend on the AODs and AOAs for the LOS and NLOS paths according to (1). Moreover, as presented in section II, by geometrical analysis, there exists a relation between the known location of D1, the unknown position of D2 with the AOD, $\theta_{\text{tx},0}$, the AOA $\theta_{\text{rx},0}$ and the delay τ_0 for the LOS path. Similarly, for the k-th NLOS path, there exists a relation between the incidence point location $\mathbf{s}_k$ and the locations of D1, D2 by means of the delay τ_k, AOD $\theta_{\text{tx},k}$, and AOA $\theta_{\text{rx},k}$, $k \geq 1$. Given the observation model, we stack the $5K$ unknown channel parameters in the vector

$$\boldsymbol{\eta} = \left[\tau_0, \boldsymbol{\theta}_0^{\text{T}}, \mathbf{h}_0^{\text{T}}, \ldots, \tau_{K-1}, \boldsymbol{\theta}_{K-1}^{\text{T}}, \mathbf{h}_{K-1}^{\text{T}} \right]^{\text{T}},$$

where $\boldsymbol{\theta}_k = \left[\theta_{\text{tx},k}, \theta_{\text{rx},k} \right]^{\text{T}}$, $\mathbf{h}_k = \left[h_{R,k}, h_{I,k} \right]^{\text{T}} = [\Re\{h_k\}, \Im\{h_k\}]^{\text{T}}$. Moreover, here exists an injective relation from

$$\boldsymbol{\eta}' = \left[\boldsymbol{\beta}^{\text{T}}, \mathbf{h}_0^{\text{T}}, \mathbf{s}_1^{\text{T}}, \mathbf{h}_1^{\text{T}}, \ldots, \mathbf{s}_{K-1}^{\text{T}}, \mathbf{h}_{K-1}^{\text{T}} \right]^{\text{T}},$$

to $\boldsymbol{\eta}$, where $\boldsymbol{\beta} = [\mathbf{p}, \alpha]^{\text{T}}$, which will be useful in the fundamental performance characterization. Hence, since the received signals can be expressed as a function of $\boldsymbol{\eta}'$, they provide information regarding $[\mathbf{p}, \alpha]^{\text{T}}$ as well as $\mathbf{s}_k$, $k \geq 1$.

B. FUNDAMENTAL PERFORMANCE CHARACTERIZATION

In this subsection, we analyze the ability of D2 to estimate its position and orientation $\boldsymbol{\beta} = [\mathbf{p}, \alpha]^{\text{T}}$ at each iteration. The Fisher information matrix (FIM) serves as a tool to assess the quality of the estimation [42], without the need to consider a specific estimator. The FIM associated with observation $\mathbf{y}_{l,m}^{\text{T}(i)}[n]$, due to a beam pair $(\mathbf{f}_m, \mathbf{w}_l)$ subcarrier n at iteration i, and unknown vector parameter $\boldsymbol{\eta}$, $\mathbf{J}_{\boldsymbol{\eta}}^{m,l,i}[n]$, is a $5K \times 5K$ matrix, whose expression is provided in (36) in Appendix B. Due to the additive nature of Fisher information and the fact that observations are independent across subcarriers n and beam pairs, the FIM for multiple beams decouples into the sum of the corresponding FIMs over the total number of beam pairs and subcarriers. The total FIM after i iterations can then be expressed as

$$\mathbf{J}_{\boldsymbol{\eta}}^{(i)} = \sum_{i'=1}^{i} \sum_{m=1}^{M_t^{(i')}} \sum_{l=1}^{M_r^{(i')}} \sum_{n=0}^{N_s-1} \mathbf{J}_{\boldsymbol{\eta}}^{m,l,i'}[n]. \quad (9)$$

Given the injective relation between $\boldsymbol{\eta}$ and $\boldsymbol{\eta}'$ described in section IV-A, we can also determine the FIM of $\mathbf{J}_{\boldsymbol{\eta}'}^{(i)}$ as $\mathbf{J}_{\boldsymbol{\eta}'}^{(i)} = \mathbf{T}^{\text{T}} \mathbf{J}_{\boldsymbol{\eta}}^{(i)} \mathbf{T}$, where $\mathbf{T}$ is the Jacobian matrix associated with the transformation from $\boldsymbol{\eta}$ to $\boldsymbol{\eta}'$, that is, $T_{ij} = \partial \eta_i / \partial \eta'_j$. Finally, the inverse of the FIM can be related to the mean squared error (MSE) of unbiased estimators of $\boldsymbol{\eta}'$ [42]:

$$\mathbb{E}_{\mathbf{y}|\boldsymbol{\eta}'} \left[\left(\hat{\boldsymbol{\eta}}' - \boldsymbol{\eta} \right) \left(\hat{\boldsymbol{\eta}}' - \boldsymbol{\eta} \right)^{\text{T}} \right] \succeq \left[\mathbf{J}_{\boldsymbol{\eta}'}^{(i)} \right]^{-1}. \quad (10)$$

At sufficient high SNR, and under some mild conditions [43], the covariance of the maximum likelihood estimator is tight to this lower-bound. Since we operate in an indoor environment with relatively small distances, we assume the receiver operates in a high SNR regime. From this relationship, we can derive the position error bound (PEB) as

$$\text{PEB}^{(i)} = \sqrt{\text{tr} \left\{ \left[\mathbf{J}_{\boldsymbol{\eta}'}^{(i)} \right]_{1:2,1:2}^{-1} \right\}} \quad (11)$$

$$\leq \sqrt{\mathbb{E}\{\|\mathbf{p} - \hat{\mathbf{p}}\|^2\}} \quad (12)$$

and the rotation error bound (REB)

$$\text{REB}^{(i)} = \sqrt{\left[\mathbf{J}_{\boldsymbol{\eta}'}^{(i)} \right]_{3,3}^{-1}} \quad (13)$$

$$\leq \sqrt{\mathbb{E}\{\|\alpha - \hat{\alpha}\|^2\}}, \quad (14)$$

where $[\cdot]_{1:2,1:2}^{-1}$ denotes the 2×2 upper left submatrix of the inverse of the argument, and $[\cdot]_{3,3}^{-1}$ denotes the third diagonal element of the inverse of the argument. We observe that the PEB and REB must be decreasing functions of i, as progressively more information is collected.

C. POSITION AND ORIENTATION ALGORITHMS

Based on $\mathbf{y}_{l,m}^{\text{T}(i)}[n]$, $i' = 1, \ldots, i$, $n = 0, \ldots, N_s - 1$, an estimation problem can be set up to infer $\boldsymbol{\beta}$, the position and orientation of D2 at iteration i. Different approaches can be categorized into:

1) *One-step:* the location of the receiver is estimated directly from the transmitted signal, without estimating intermediate parameters, i.e., AOAs, AODs of LOS or NLOS paths [44]–[47].

2) *Two-step:* first the intermediate parameters such as AOD and AOA and delay are estimated, possibly exploiting channel sparsity [48]–[52], based upon which a position and orientation estimate is determined [12], [17], [53].

As in [37], we abstract our work from the specific method and instead assume that the estimator of D2's position and orientation at each iteration i is efficient, i.e., (i) it is unbiased, (ii) the MSE is close to the PEB and the REB at medium to high SNRs. Hence, we assume an idealized receiver which serves to understand the potential behind the use of position information in the initial access procedure and thus provides a bound for any real receiver. We denote the estimate of $\boldsymbol{\beta}$ at
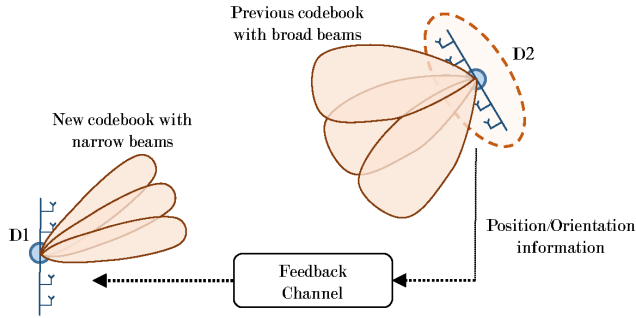
FIGURE 2. High level depiction of the joint positioning and beam selection protocol. Position and orientation information are fed back from D2 to D1. This information is used by D1 to select a higher directivity codebook to refine beam search alignment.

iteration i by $\hat{\boldsymbol{\beta}}^{(i)}$, with associated covariance matrix

$$\boldsymbol{\Sigma}_{\boldsymbol{\beta}}^{(i)} = \left[\mathbf{J}_{\boldsymbol{\eta}'}^{(i)}\right]_{1:3,1:3}^{-1}. \tag{15}$$

Remark 1: The approach's main goal is the estimate of the position and orientation of D2. However, as a side product, estimates of the incidence point can be obtained. Both Bayesian [53] and non Bayesian [17] methods exist, which include the ability to estimate the number of paths. These estimates can be used to optimize beam alignment, since beams can be pointed towards the point scatterers themselves. This kind of optimization is relevant when D1, and D2 have more than one radio frequency chain, and when the LOS is obstructed between devices, so that the best NLOS path is discovered.

V. JOINT POSITIONING AND BEAM SELECTION PROTOCOL

In this section, we propose an iterative positioning-based beam selection protocol compatible with the conventional protocol from section III, but including the ability to reduce the initial access time by exchanging in-band position information, obtained as described in section IV. Hence, after initial access, we aim to have a high SNR for communication and a low error in the estimate of the position and orientation of D2.

A. PROTOCOL DESCRIPTION

The joint positioning and beam selection protocol is an iterative procedure that harnesses not only the received powers at D2, but also its estimated position and orientation $\hat{\boldsymbol{\beta}} = [\hat{\mathbf{p}}, \hat{\alpha}]^{\mathrm{T}}$. First, at every iteration i the transmitter sends a training OFDM signal $\mathbf{x}[n]$ over N_s subcarriers for all the $M_t^{(i)} \times M_r^{(i)}$ pairs $(\mathbf{f}_m, \mathbf{w}_l)$. The receiver D2 computes the corresponding received energy for each beam pair and gathers them in the matrix $\mathbf{P}^{(i)} \in \mathbb{R}^{M_t^{(i)} \times M_r^{(i)}}$. Moreover, D2 determines an estimate of its position as described in section IV-C. Considering the position and orientation estimation are well approximated by the Gaussian distribution with mean $\hat{\boldsymbol{\beta}}^{(i)}$ and a covariance matrix $\boldsymbol{\Sigma}_{\boldsymbol{\beta}}^{(i)}$. This information can be used not only by D2 but is also fed back to D1. As a consequence,

---

Algorithm 1 Joint Positioning and Beam Selection

Input: $N_t^{'(1)}$, M_t, $f_{\mathrm{map}}^{\mathrm{tx}}$, $N_r^{'(1)}$, M_r, $f_{\mathrm{map}}^{\mathrm{rx}}$, N_t, and N_r

while $N_t^{'(i)} \leq N_t$ or $N_r^{'(i)} \leq N_r$ **do**
  for $m = 1$ to $M_t^{(i)}$ **do**
    for $l = 1$ to $M_r^{(i)}$ **do**
      D1 transmits a training sequence for each m-th beam pattern, $\mathbf{f}_m^{(i)}$;
      D2 measures received power $P_{l,m}^{(i)} = \sum_{n=0}^{N_s-1} \left\| \mathbf{y}_{l,m}^{\mathrm{T}(i)}[n] \right\|^2$ for the m-th transmit pattern with its l-th receive pattern $\mathbf{w}_l^{(i)}$;
    end for
  end for
  D2 performs in-band positioning and determines a position estimate and uncertainty $[\hat{\boldsymbol{\beta}}^{(i)}, \boldsymbol{\Sigma}_{\boldsymbol{\beta}}^{(i)}]$;
  D2 feeds back $[\mathbf{P}^{(i)}, \hat{\boldsymbol{\beta}}^{(i)}, \boldsymbol{\Sigma}_{\boldsymbol{\beta}}^{(i)}]$ to D2;
  $i = i + 1$;
  A new selection of beams is obtained for
  D1: $\mathcal{F}^{(i)} = f_{\mathrm{map}}^{\mathrm{tx}}(\mathcal{F}^{(i-1)}, \mathbf{P}^{(i-1)}, \hat{\boldsymbol{\beta}}^{(i-1)}, \boldsymbol{\Sigma}_{\boldsymbol{\beta}}^{(i-1)})$;
  D2: $\mathcal{W}^{(i)} = f_{\mathrm{map}}^{\mathrm{rx}}(\mathcal{W}^{(i-1)}, \mathbf{P}^{(i-1)}, \hat{\boldsymbol{\beta}}^{(i-1)}, \boldsymbol{\Sigma}_{\boldsymbol{\beta}}^{(i-1)})$;
end while
Output: Final transmit and receive beam pattern selections $\mathbf{f}_{\mathrm{sel}}$, and $\mathbf{w}_{\mathrm{sel}}$.

---

adaptive mapping functions $f_{\mathrm{map}}^{\mathrm{tx}}$, and $f_{\mathrm{map}}^{\mathrm{rx}}$ can be designed to compute the new number of active antennas as well as the new set of beams $\mathcal{F}^{(i)} = f_{\mathrm{map}}^{\mathrm{tx}}(\mathcal{F}^{(i-1)}, \mathbf{P}^{(i-1)}, \hat{\boldsymbol{\beta}}^{(i-1)}, \boldsymbol{\Sigma}_{\boldsymbol{\beta}}^{(i-1)})$ and $\mathcal{W}^{(i)} = f_{\mathrm{map}}^{\mathrm{rx}}(\mathcal{W}^{(i-1)}, \mathbf{P}^{(i-1)}, \hat{\boldsymbol{\beta}}^{(i-1)}, \boldsymbol{\Sigma}_{\boldsymbol{\beta}}^{(i-1)})$ for beamforming at D1 and D2, respectively. Examples of mapping functions will be presented later in the paper. The protocol is described in Algorithm 1.

B. CHOICE OF MAPPING

The mapping functions at transmitter and receiver account both for the receiver energies at D2 as well as the estimation position and orientation. While a variety of mapping functions are possible, we here focus on reducing the set-up time by allowing larger increases in the number of active antennas and avoiding making incorrect beam decisions.

- *D1 operation:* When the position information is sufficiently accurate, this allows D1 to select a codebook (from the conventional protocol) with higher directivity, thus selecting a value of $N_t^{'(i)}$ that can significantly exceed $2N_t^{'(i-1)}$, as described in [37]. Given $\hat{\boldsymbol{\beta}}^{(i-1)}$, $\boldsymbol{\Sigma}_{\boldsymbol{\beta}}^{(i-1)}$, D1 determines the AOD estimate $\hat{\theta}_{\mathrm{tx}}^{(i-1)}$ and uncertainty (standard deviation) $\sigma_{\mathrm{tx}}^{(i-1)}$. Then D1 solves the following problem

$$\text{maximize } N_t^{'(i)} \tag{16}$$

$$\text{subject to } \mathbf{f} = \arg\max_{\tilde{\mathbf{f}} \in \mathcal{C}_{\mathrm{tx}}(N_t^{'(i)})} \left| \mathbf{a}_{\mathrm{tx}}^{\mathrm{H}}(\hat{\theta}_{\mathrm{tx}}^{(i-1)})\tilde{\mathbf{f}} \right| \tag{17}$$

$$\kappa \sigma_{\text{tx}}^{(i-1)} \leq 3\theta_{\text{HPBW}}(\mathbf{f}) \tag{18}$$

$$N_t'^{(i)} \geq \zeta N_t'^{(i-1)} \tag{19}$$

where $\zeta > 1$ is a design parameter to ensure sufficient progress, while $\kappa > 1$ is set to attain a certain level of robustness against the positioning error, and $\theta_{\text{HPBW}}(\mathbf{f})$ returns the half-power beamwidth angle of the beam $\mathbf{f}$ using $N_t'^{(i)}$ active antennas. When the problem (16) is not feasible, D1 sets $N_t'^{(i)} = N_t'^{(i-1)}$ in order to collect more information. Solving the optimization problem entails limited complexity: for a fixed value of $N_t'^{(i)}$, finding $\mathbf{f}$ is straightforward as it can be implemented in a table look-up. Verifying the remaining constraints is trivial.

- *D2 operation:* Independent of D1, D2 solves a similar optimization problem based on $\mathbf{w} = \arg\max_{\tilde{\mathbf{w}} \in \mathcal{C}_{\text{rx}}(N_r'^{(i)})} \left| \tilde{\mathbf{w}}^{\text{H}} \mathbf{a}_{\text{rx}}(\hat{\theta}_{\text{rx}}^{(i-1)}) \right|$ in order to find the largest possible value of $N_r'^{(i)}$.

Setting a larger ζ avoids making small increments in the number of active antennas, while larger κ means that we want to cover the angle uncertainty sufficiently well with 3 beams.

VI. PERFORMANCE METRICS

In this section, we present the performance metrics for the protocols presented in sections III and V. The goal of the protocols is to reliably determine the precoding matrix $\mathbf{f}_{\text{sel}}$ and the combining matrix $\mathbf{w}_{\text{sel}}$ in a fast manner. Hence, the relevant performance metrics include: SNR, positioning quality computed after beam alignment and delay.

1) **SNR:** The selection of $\mathbf{f}_{\text{sel}}$ and $\mathbf{w}_{\text{sel}}$ has as main objective to maximize the SNR, which is defined as

$$\text{SNR} \triangleq \frac{E_x}{N_0 N_s} \sum_{n=0}^{N_s-1} |\mathbf{w}_{\text{sel}}^{\text{H}} \mathbf{H}[n] \mathbf{f}_{\text{sel}}|^2, \tag{20}$$

where E_x is the energy per symbol.

2) **Positioning quality:** The MSE of the positioning and orientation errors are

$$\mathbb{E}\{\|\mathbf{p} - \hat{\mathbf{p}}\|^2\} \tag{21}$$

and

$$\mathbb{E}\{\|\alpha - \hat{\alpha}\|^2\}, \tag{22}$$

where $\hat{\mathbf{p}}$ and $\hat{\alpha}$ denote the estimated position and angle of rotation for the D2, respectively, obtained from the sequence of received signals of the form (5).

3) **Delay:** Assuming a fixed number[2] of symbols and subcarriers throughout each iteration i, the delay is dependent on the number of $M_t \times M_r$ pairs $(\mathbf{f}_m, \mathbf{w}_l)$, the number of subcarriers N_s employed and number of symbols sent $N^{(i)}$. The number of OFDM symbols $N^{(i)}(N_t', N_r', \varepsilon)$ at each iteration is predefined and

---

[2] More advanced protocols can include adaptive number of symbols and subcarriers within each iteration to mitigate beam alignment errors and reduce even further the delay.

dependent on the number of active transmitting, receiving antennas and the alignment error probability ε and the same for all protocols. Thus, the delay at the final iteration I can be defined as the total number of OFDM symbols transmitted as:

$$D = N_s \sum_{i=1}^{I} N^{(i)} M_t^{(i)} M_r^{(i)}. \tag{23}$$

VII. SIMULATION RESULTS

A. SIMULATION SETUP

D1 is fixed at position $\mathbf{q} = [0, 0]^{\text{T}}$ and D2 located at $\mathbf{p} = [7, 4]^{\text{T}}$. We assume $K = 2$ paths are possible by considering the existence of a reflector, represented as a line between points $[5, 5]^{\text{T}}$ and $[5, 7]^{\text{T}}$. If D2 is inside the reflective area then an incidence point is located at $\mathbf{s} = [s_x, s_y]^{\text{T}}$, where $\{s_x \mid 5 \leq s_x \leq 7\}$ and $s_y = 5$. The ULAs are along the vertical axis. We set for the LOS path

$$h_0 = \sqrt{(1 - \xi)^2} \exp(j\phi_0)/\sqrt{\rho_0}, \tag{24}$$

where $\rho_0 = (2\pi \|\mathbf{q} - \mathbf{p}\|/\lambda)^2$ is the path-loss between D1 and D2, $\phi_0 \sim \mathcal{U}(0, 2\pi)$ and $\xi \in [0, 1]$. For the NLOS path, we set

$$h_k = \sqrt{\xi^2} \exp(j\phi_k)/\sqrt{\rho_k} \tag{25}$$

where $\rho_k = (\Gamma 2\pi(\|\mathbf{q} - \mathbf{s}_k\| + \|\mathbf{s}_k - \mathbf{p}\|)/\lambda)^2$, Γ is the reflection coefficient and $\phi_1 \sim \mathcal{U}(0, 2\pi)$. When the NLOS path corresponds to a cluster of unresolved rays, the value of h_k should be replaced by the superposition of the complex gains of each ray. The parameter ξ allows us to control the energy division between the LOS and NLOS paths, i.e., when $\xi = 0$, only the LOS path is present, while when $\xi = 1$ only the NLOS path is present. Moreover, we set $f_c = 60$ GHz, $B = 100$ MHz, and a nominal SNR of 10 dB at a distance of 10 meters between D1 and D2 for a fixed $\xi = 0.25$. Furthermore, we consider $N_s = 65$ subcarriers, the number of antennas at both D1 and D2 is $N_t = N_r = 64$, and the inter-element spacing is $d = \lambda/2$. The number of OFDM symbols $N^{(i)}(N_t'^{(i)}, N_r'^{(i)}, \varepsilon)$ are tabulated and equally defined for all protocols.

We will evaluate three protocols in terms of SNR, positioning and orientation quality (PEB and REB) and delay for scenarios with the reflector (R) and with no reflector (NR):

- *Conventional beam selection protocol* (CBS) which can only use $M_t, M_r \in \{2, 4, 8, 16, 32, 64\}$ discrete beams, $N_t' = M_t$ and $N_r' = M_r$ active contiguous antennas sequentially selected, generated using phase shifters $\phi_i = \{\pi, 0, \pi/2, -\pi/2\}$, based on [8]. The CBS is instantiated according to the hierarchical approach described in section III-C.

- *Joint positioning and beam selection protocol* (JPBS), which uses the same discrete codebook as the CBS. The JPBS generates estimates of the position of D2 as $\hat{\mathbf{p}} \sim \mathcal{N}(\mathbf{p}, [\mathbf{J}_{\eta'}^{(i)}]_{1:2,1:2}^{-1})$ where $[\cdot]_{1:2,1:2}^{-1}$ denotes the 2×2 upper left submatrix of the inverse of the argument. The JPBS

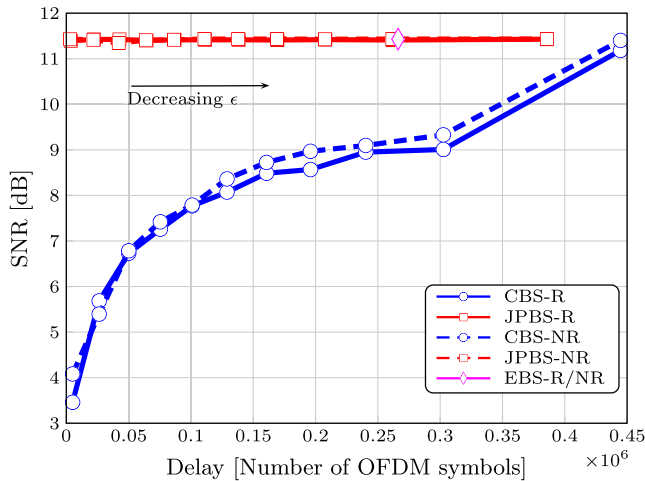**FIGURE 3.** SNR as a function of the total number of OFDM symbols.

FIGURE 4. PEB as a function of the total number of OFDM symbols.

is instantiated as described in section V. The design parameters are set to $\zeta = 2$ and $\kappa = 2$.

- For the sake of completeness we include results for an *exhaustive beam selection* (EBS) protocol instantiated as explained in section III-C.

We note that since both the devices have a single RF chain, comparison with more sophisticated protocols (e.g., with hybrid precoding) is not possible.

B. RESULTS AND DISCUSSION

1) SNR VS. DELAY

Figure 3 shows the final SNR, as expressed in equation (20), as a function of the total number of total OFDM symbols needed for the protocols for $\xi = 0.25$ for different values of ε (ranging from 0.5 on the left side to 0.01 on the right side). A lower ε requires a higher number of transmitted symbols $N^{(i)}$ to attain the desired alignment error requirement. The exhaustive protocol corresponds to a single delay, since $N^{(i)}(N_t'^{(i)} = 64, N_r'^{(i)} = 64, \varepsilon) = 1$, and thus shows as a single point in the figure. As expected, we observe that for the CBS protocol the SNR increases with smaller ε. However, the SNR increase comes at a cost in terms of delay since a lower ε leads to more OFDM symbols per iteration. The JPBS shows a constant maximum achievable SNR. The SNR of the positioning-based protocol is not affected by ε, instead, a lower ε allows the JPBS to collect more information at early iterations since a higher number of OFDM symbols are transmitted, and thus perform aggressive increases at each iteration on the number of active contiguous antennas at the transmitter and receiver, $N_t'^{(i)}$ and $N_r'^{(i)}$, respectively. These aggressive increases translate into a smaller delay for a given value of ε compared to the CBS. The JPBS protocol attains to the achievable SNR even for a high ε at a small delay compared to the CBS and at more than a hundred times faster. Note that, it is only when $\varepsilon \approx 0.01$ (right-most markers) that the SNR for both the conventional and the positioning protocol are the same achievable SNR.
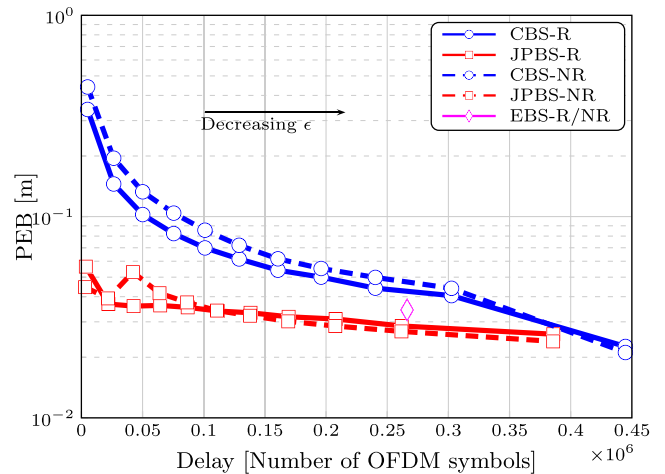
2) POSITIONING ERROR VS. DELAY

Figure 4 shows the PEB as a function of the total number OFDM symbols for a fixed $\xi = 0.25$. Note that in practice, position information can only be exploited by the JPBS. Once again, for each protocol line in Figure 4 the markers to the left-most correspond to the probability of making a mistake in the beam pair selection half of the time, i.e., $\varepsilon = 0.5$, while the markers at the right-most of the plot for each of the protocol lines correspond to a low probability of making a mistake, i.e., $\varepsilon = 0.01$. The exhaustive approach exhibits a fixed number of OFDM transmitted symbols. Since for a fixed ε there exists a fixed number of OFDM symbols transmitted per beam pair combination the PEB remains fixed due to the fact that the FIM always harnesses the same information. We can observe for the conventional approach that the PEB decreases with decreasing ε: lower alignment error probability results in less beams pair misalignment within iterations, which in turn affects the positioning error. Similar behavior for the REB occurs, thus, only figures for the PEB are included. Under the same initial conditions, the JPBS shows lower PEB even in scenarios with large alignment error probability. For instance, for $\varepsilon = 0.35$ the PEB for the JPBS is approximately 55% and 65% lower in comparison with the CBS-NR and CBR-R, respectively; while the delay is approximately 15% lower, respectively. As discussed before, ε has no direct impact on the JPBS protocol in terms of final SNR. However, a change in ε involves a change in the number of iterations and thus, transmitted OFDM symbols, which affect the position estimation. Figs. 6 and 7 exemplify the convergence of the JPBS in terms of the probability of change of the selected number of active antennas for the transmitting and receiver devices for $\epsilon = 0.5$. As an example, in Fig. 6, there is probability of 0.41 and 0.55 to go from 2 transmitting antennas at iteration i to 8 or 16 antennas at iteration $i+1$, respectively. Similarly, there exists approximately a probability of 0.85 when going from 8 or 16 active transmitting antennas to at iteration i to 64 antennas at iteration $i+1$. We can observe that despite the high beam alignment the JPBS protocol shows a fast convergence
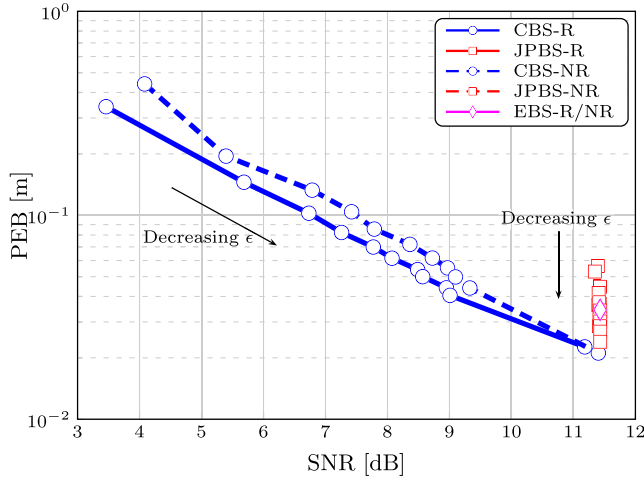
FIGURE 5. PEB as a function of the final SNR. Different data points correspond to different values of ε, where smaller ε leads to higher SNR and lower PEB at a cost of more delay. The proposed JPBS method achieves the highest SNR.
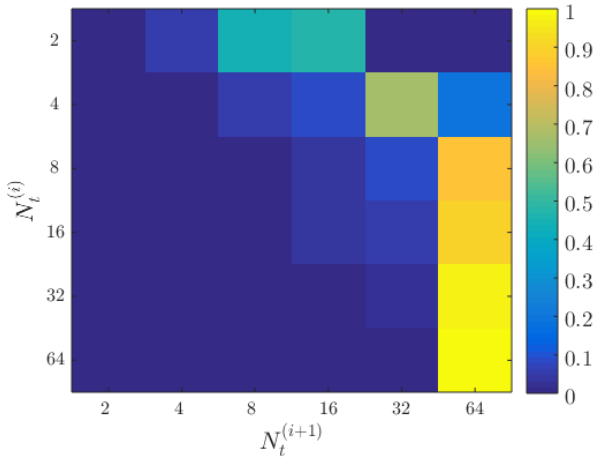

FIGURE 7. Probability of the change of selected number of receiving active antennas antennas from iteration i to iteration $i + 1$ for $\epsilon = 0.5$.

FIGURE 6. Probability of the change of selected number of transmitting active antennas from iteration i to iteration $i + 1$ for $\epsilon = 0.5$.

FIGURE 8. PEB as a function of the final SNR for different LOS and NLOS conditions for $\varepsilon = 0.1$. Different data points correspond to different ξ, where increasing ξ means a weaker LOS and a stronger NLOS path. The conventional methods are more robust than the proposed method, leading to high SNR when all the energy is in a single path (LOS or NLOS).

in terms of the number of selected active antennas between consecutive iterations.

3) SNR VS. POSITIONING ERROR

Figure 5 shows the connection between SNR and PEB for the different protocols and a fixed $\xi = 0.25$. Each marker within each protocol's curve corresponds to a different ε. The EBS protocol shows a fixed SNR and PEB independent of the alignment error probability. We observe that for the CBS protocol a low PEB means a higher SNR, since at small alignment error probabilities, beam pairs within each iteration are correctly chosen to be aligned between devices, contributing to a lower PEB. Finally, the JPBS shows a PEB decrease for decreasing ε. For each protocol, attaining better SNR and lower PEB are a consequence of devoting more time during initial access. Hence, there is no trade-off between communication and localization performance.
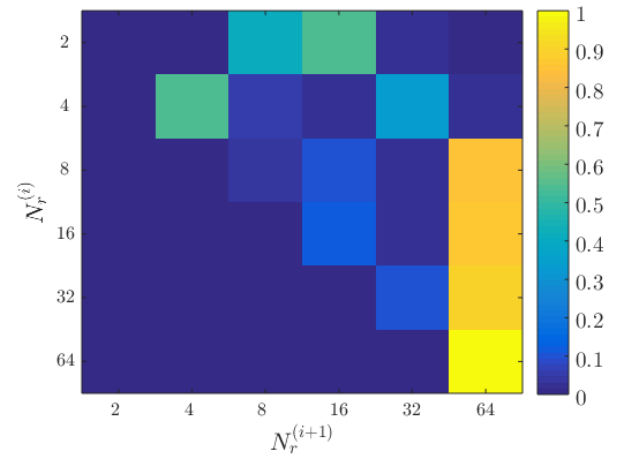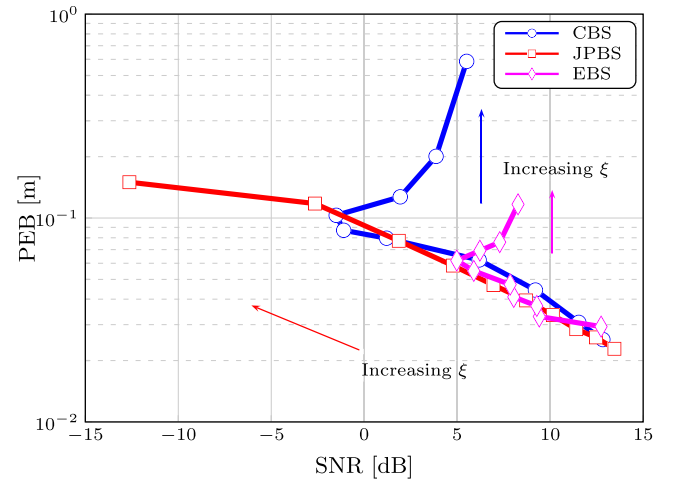
4) LOS VS. NLOS

In contrast to [54], which considered a trade off between PEB and effective rate, rather than SNR, Figure 8 shows the relationship between the SNR and PEB for different LOS and NLOS conditions for a fixed $\varepsilon = 0.1$. Each marker within the protocol's curve corresponds to a increasing ξ, where $\xi = 0$ corresponds to the existence only of the LOS path component, and $\xi = 1$ corresponds to the existence only of the reflected path. The JPBS shows a negative linear trend with increasing ξ, showing that both the PEB and SNR of the JPBS degrade when ξ approaches 1, since JPBS is designed specifically for channels with a strong LOS component (see also Figure 9). The CBS and EBS show a similar behavior: when $\xi \approx 1$ a lower SNR is achieved compared to the case where only a LOS path exists, i.e., $\xi = 0$, due to the higher pathloss. Moreover, both methods show their higher PEB and lowest SNR when $\xi \approx 0.55$, when the reflected path is just slightly stronger than the LOS path.
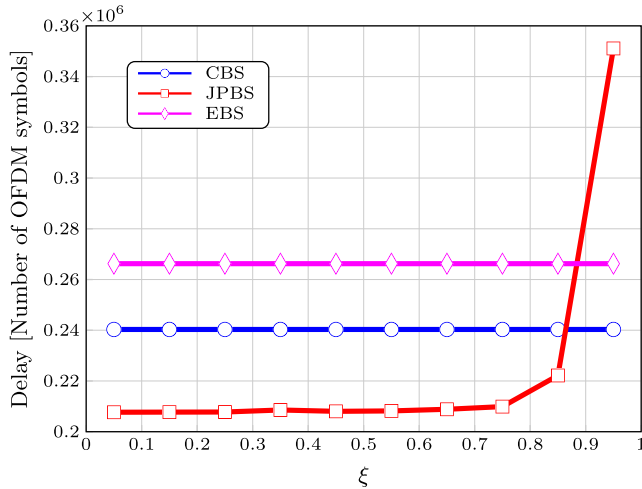
FIGURE 9. Number of OFDM symbols as a function of LOS and NLOS energy parameter ξ, for a fixed $\epsilon \approx 0.1$.

For $\xi > 0.55$, the EBS and CBS are able to partially recover their SNR performance by beaming towards the incidence point.

Finally, Figure 9 depicts the delay as a function of the LOS and NLOS conditions. Note that for $0 \leq \xi \leq 0.75$ the JPBS protocol shows a reduction in the delay of approximately 14% and 22% compared to the CBS and EBS, respectively. However, for a $\xi \approx 1$, the JPBS needs a larger number of transmitted symbols due to the poor position estimates which translate into a higher delay compared to both the CBS and EBS.

We can conclude that under a small and fixed ε and a strong LOS path, all protocols have a similar SNR performance but the JPBS outperforms the other protocols in terms of delay, which results in faster set up times; on the other hand when the NLOS path is strong (ii) the CBS and EBS show an overall better performance in terms of delay and SNR compared to the JPBS, which due to the poor position estimates require a high number of iterations and is not able to establish a reliable link.

VIII. CONCLUSION

We have proposed and analyzed a novel simultaneous positioning and beam selection protocol, harnessing the synergy between communication and positioning that exists in mm-wave channels. We have shown that an in-band position-aided protocol achieves similar, or even better, SNR as the conventional protocol but with a reduction of the setup time. This improved performance comes at a cost of increased computational complexity, as at each iteration the position and orientation of a device needs to be estimated. The provided position information is more accurate than in the conventional protocol. Moreover, for short durations of the reference signal, the conventional protocol is prone to beam alignment errors, and the positioning-aided protocol outperforms the conventional protocols in terms of final SNR at a similar performance in delay. The position-aided protocol can operate in

the presence of multipath propagation channels, provided the LOS path is sufficiently strong compared to other paths. The protocol can be extended to explicitly account for multipath (through estimating incidence points) as well, in order to operate when LOS is weak or not present.

APPENDIX A
ALIGNMENT ERROR AND NUMBER OF SYMBOLS

In order to set the number of OFDM symbols N at each iteration i we observe that the received signal $Y_{l,m} \doteq \sum_{n=0}^{N_s-1} \left\| \mathbf{y}_{l,m}^{\mathrm{T}}[n] \right\|^2$ exhibits a non-central chi-squared random distribution with non-centrality parameter $v_{l,m}$ from (6) and $k = NN_s$ degrees of freedom, i.e., $Y_{l,m} \sim \chi^2_{NN_s}(v_{l,m})$. Following the central limit theorem, the received signal can be approximated as a Gaussian random variable [55]

$$\frac{Y_{l,m}}{NN_s} \sim \mathcal{N}\left(1 + v_{l,m}, \frac{2(1 + v_{l,m})}{NN_s}\right) \qquad (26)$$

We can express the alignment error probability ε (at iteration i) as

$$\varepsilon = \Pr(\cup_{[l,m]} Y_{l,m} > Y_{l^*,m^*}) \qquad (27)$$

$$\leq \sum_{l,m} \Pr(Y_{l,m} > Y_{l^*,m^*}) \qquad (28)$$

$$\approx \Pr(Y_{l^*-1,m^*} > Y_{l^*,m^*}) + \Pr(Y_{l^*,m^*-1} > Y_{l^*,m^*}) \qquad (29)$$
$$+ \Pr(Y_{l^*+1,m^*} > Y_{l^*,m^*}) + \Pr(Y_{l^*,m^*+1} > Y_{l^*,m^*}),$$

The inequality in equation (28) follows from the union union bound and the approximation in (29) reflects the error being dominated by neighboring beams. Given the symmetry within the codebook design we can express ϵ as

$$\varepsilon \approx 2\Pr(Y_{l^*-1,m^*} - Y_{l^*,m^*} > 0)$$
$$+ 2\Pr(Y_{l^*,m^*-1} - Y_{l^*,m^*} > 0) \qquad (30)$$

We note that when $N_t' > N_r'$, then the first term in (30) will dominate (as the receiver is using broader beams and is thus more likely to make errors), while for $N_t' < N_r'$, the second term in (30) will dominate. From (26), we find that

$$Y_{l,m}/(NN_s) - Y_{l^*,m^*}/(NN_s) \sim \qquad (31)$$

$$\mathcal{N}\left(\underbrace{v_{l,m} - v_{l^*,m^*}}_{<0}, \frac{2(2 + v_{l,m} + v_{l^*,m^*})}{NN_s}\right),$$

from which it follows that

$$\Pr(Y_{l^*-1,m^*}/(NN_s) - Y_{l^*,m^*}/(NN_s) > 0) \qquad (32)$$
$$= Q\left(\frac{\sqrt{NN_s}(v_{l^*,m^*} - v_{l^*-1,m^*})}{\sqrt{2(2 + v_{l^*-1,m^*} + v_{l^*,m^*})}}\right)$$

$$\Pr(Y_{l^*,m^*-1}/(NN_s) - Y_{l^*,m^*}/(NN_s) > 0) \qquad (33)$$
$$= Q\left(\frac{\sqrt{NN_s}(v_{l^*,m^*} - v_{l^*,m^*-1})}{\sqrt{2(2 + v_{l^*,m^*-1} + v_{l^*,m^*})}}\right) \qquad (34)$$

where $Q(\cdot)$ denotes the Q-function. Hence,

$$
\varepsilon \approx
\begin{cases}
2Q\left(\dfrac{\sqrt{NN_s}(\nu_{l^*,m^*} - \nu_{l^*-1,m^*})}{\sqrt{2(2 + \nu_{l^*-1,m^*} + \nu_{l^*,m^*})}}\right) & N_t' > N_r' \\[2ex]
2Q\left(\dfrac{\sqrt{NN_s}(\nu_{l^*,m^*} - \nu_{l^*,m^*-1})}{\sqrt{2(2 + \nu_{l^*,m^*-1} + \nu_{l^*,m^*})}}\right) & N_t' < N_r' \\[2ex]
4Q\left(\dfrac{\sqrt{NN_s}(\nu_{l^*,m^*} - \nu_{l^*-1,m^*})}{\sqrt{2(2 + \nu_{l^*-1,m^*} + \nu_{l^*,m^*})}}\right) & N_t' = N_r'
\end{cases}
$$

from which solving for NN_s immediately leads to (8).

APPENDIX B
DERIVATION OF THE FIM
We consider the case of multiple paths under OFDM transmission and a transmitting $\mathbf{f}_m \in \mathcal{C}_{\text{tx}}$ and and a receiving beam $\mathbf{w}_l \in \mathcal{C}_{\text{rx}}$. Without loss of generality, we do not include the subscripts of the beam pair for simplicity in the derivation. The general form of the FIM for k paths and subcarrier n is given by

$$
\mathbf{J}_\eta[n] =
\begin{bmatrix}
\mathbf{J}_{(1,1)}[n] & \cdots & \mathbf{J}_{(1,k)}[n] \\
\vdots & \ddots & \vdots \\
\mathbf{J}_{(k,1)}[n] & \cdots & \mathbf{J}_{(k,k)}[n]
\end{bmatrix}, \tag{36}
$$

where each of the sub-matrices has the form (35), as shown at the top of the next page. Denoting the noise-free signal by

$$
\mathbf{m}[n] = \sum_{k=0}^{K-1} \mathbf{w}^H \mathbf{H}_k[n] \mathbf{f} \mathbf{x}^T[n], \tag{37}
$$

it can be shown that

$$
\Phi(x_1, x_2) = \frac{2}{N_0} \Re\left\{\int \frac{\partial \mathbf{m}^H[n]}{\partial x_1} \frac{\partial \mathbf{m}[n]}{\partial x_2} dt\right\}. \tag{38}
$$

We define $\kappa = \sqrt{N_t N_r}$ and it is readily verified that for an arbitrary path i,

$$
\frac{\partial \mathbf{m}[n]}{\partial \tau_i}
$$
$$
= \kappa h_i \exp\left(\frac{-j2\pi n \tau_i}{NT_s}\right) \frac{-j2\pi n}{NT_s} \mathbf{w}^H \mathbf{a}_{\text{rx}}(\theta_{\text{rx},i}) \mathbf{a}_{\text{tx}}^H(\theta_{\text{tx},i}) \mathbf{f} \mathbf{x}[n] \tag{39}
$$

$$
\frac{\partial \mathbf{m}[n]}{\partial \theta_{\text{tx},i}}
$$
$$
= \kappa h_i \exp\left(\frac{-j2\pi n \tau_i}{NT_s}\right) \mathbf{w}^H \mathbf{a}_{\text{rx}}(\theta_{\text{rx},i}) \dot{\mathbf{a}}_{\text{tx}}^H(\theta_{\text{tx},i}) \mathbf{f} \mathbf{x}[n] \tag{40}
$$

$$
\frac{\partial \mathbf{m}[n]}{\partial \theta_{\text{rx},i}}
$$
$$
= \kappa h_i \exp\left(\frac{-j2\pi n \tau_i}{NT_s}\right) \mathbf{w}^H \dot{\mathbf{a}}_{\text{rx}}(\theta_{\text{rx},i}) \mathbf{a}_{\text{tx}}^H(\theta_{\text{tx},i}) \mathbf{f} \mathbf{x}[n] \tag{41}
$$

$$
\frac{\partial \mathbf{m}[n]}{\partial h_{R,i}}
$$
$$
= \kappa \exp\left(\frac{-j2\pi n \tau_i}{NT_s}\right) \mathbf{w}^H \mathbf{a}_{\text{rx}}(\theta_{\text{rx},i}) \mathbf{a}_{\text{tx}}^H(\theta_{\text{tx},i}) \mathbf{f} \mathbf{x}[n] \tag{42}
$$

$$
\frac{\partial \mathbf{m}[n]}{\partial h_{I,i}}
$$
$$
= \kappa j \exp\left(\frac{-j2\pi n \tau_i}{NT_s}\right) \mathbf{w}^H \mathbf{a}_{\text{rx}}(\theta_{\text{rx},i}) \mathbf{a}_{\text{tx}}^H(\theta_{\text{tx},i}) \mathbf{f} \mathbf{x}[n] \tag{43}
$$

We easily find that the diagonal elements of the submatrices $\mathbf{J}_{(i,j)}[n]$. We first define $1/\sigma^2 = 2N_r N_t / N_0$, $\gamma_{\text{tx},i} = \mathbf{f}^H \mathbf{a}_{\text{tx}}(\theta_{\text{tx},i})$, $\gamma_{\text{rx},i} = \mathbf{a}_{\text{rx}}^H(\theta_{\text{tx},i})\mathbf{w}$ as well as $\dot{\mathbf{a}}_{\text{tx}}(\theta_{\text{tx}}) = \partial \mathbf{a}_{\text{tx}}(\theta_{\text{tx}})/\partial \theta_{\text{tx}}$, $\dot{\gamma}_{\text{tx},i} = \dot{\mathbf{a}}_{\text{tx}}^H(\theta_{\text{tx},i})\mathbf{f}$, and $\dot{\gamma}_{\text{rx},i} = \mathbf{w}^H \dot{\mathbf{a}}_{\text{rx}}(\theta_{\text{tx},i})$. We also introduce $A_l[n] = (2\pi n/(NT_s))^l$, and $\Delta_{ij}[n] = \exp\left(-j2\pi n \left(\tau_i - \tau_j\right)/(NT_s)\right)$.

DIAGONAL ELEMENTS OF $\mathbf{J}_{(i,j)}$
We then find that

$$
\Phi(\tau_i, \tau_j, n)
$$
$$
= \frac{1}{\sigma^2} \Re\left\{h_i^* h_j A_2[n] \Delta_{ij}[n] \gamma_{\text{tx},i} \gamma_{\text{tx},j}^* \gamma_{\text{rx},i} \gamma_{\text{rx},j}^* \|\mathbf{x}[n]\|^2\right\} \tag{44}
$$
$$
\Phi(\theta_{\text{tx},i}, \theta_{\text{tx},j}, n)
$$
$$
= \frac{1}{\sigma^2} \Re\left\{h_i^* h_j A_0[n] \Delta_{ij}[n] \dot{\gamma}_{\text{tx},i}^* \dot{\gamma}_{\text{tx},j} \gamma_{\text{rx},i} \gamma_{\text{rx},j}^* \|\mathbf{x}[n]\|^2\right\} \tag{45}
$$
$$
\Phi(\theta_{\text{rx},i}, \theta_{\text{rx},j}, n)
$$
$$
= \frac{1}{\sigma^2} \Re\left\{h_i^* h_j A_0[n] \Delta_{ij}[n] \gamma_{\text{tx},i} \gamma_{\text{tx},j}^* \dot{\gamma}_{\text{rx},i}^* \dot{\gamma}_{\text{rx},j} \|\mathbf{x}[n]\|^2\right\} \tag{46}
$$
$$
\Phi(h_{R,i}, h_{R,j}, n) = \Phi(h_{I,i}, h_{I,j}, n)
$$
$$
= \frac{1}{\sigma^2} \Re\left\{A_0[n] \Delta_{ij}[n] \gamma_{\text{tx},i} \gamma_{\text{tx},j}^* \gamma_{\text{rx},i} \gamma_{\text{rx},j}^* \|\mathbf{x}[n]\|^2\right\}. \tag{47}
$$

OFF-DIAGONAL ELEMENTS OF $\mathbf{J}_{(i,j)}$
The off-diagonal elements are computed in similar fashion. The final expressions for the upper diagonal elements are computed as:

$$
\Phi(\tau_i, \theta_{\text{tx},j}, n)
$$
$$
= \frac{1}{\sigma^2} \Re\left\{jh_i^* h_j A_1[n] \Delta_{ij}[n] \gamma_{\text{tx},i} \dot{\gamma}_{\text{tx},j} \gamma_{\text{rx},i} \gamma_{\text{rx},j}^* \|\mathbf{x}[n]\|^2\right\} \tag{48}
$$
$$
\Phi(\tau_i, \theta_{\text{rx},j}, n) =
$$
$$
= \frac{1}{\sigma^2} \Re\left\{jh_i^* h_j A_1[n] \Delta_{ij}[n] \gamma_{\text{tx},i} \gamma_{\text{tx},j}^* \gamma_{\text{rx},i} \dot{\gamma}_{\text{rx},j} \|\mathbf{x}[n]\|^2\right\} \tag{49}
$$
$$
\Phi(\tau_i, h_{R,j}, n)
$$
$$
= \frac{1}{\sigma^2} \Re\left\{jh_i^* A_1[n] \Delta_{ij}[n] \gamma_{\text{tx},i} \gamma_{\text{tx},j}^* \gamma_{\text{rx},i} \gamma_{\text{rx},j}^* \|\mathbf{x}[n]\|^2\right\} \tag{50}
$$
$$
\Phi(\tau_i, h_{I,j}, n)
$$
$$
= -\frac{1}{\sigma^2} \Re\left\{h_i^* A_1[n] \Delta_{ij}[n] \gamma_{\text{tx},i} \gamma_{\text{tx},j}^* \gamma_{\text{rx},i} \gamma_{\text{rx},j}^* \|\mathbf{x}[n]\|^2\right\} \tag{51}
$$
$$
\Phi(\theta_{\text{tx},i}, \theta_{\text{rx},j}, n)
$$
$$
= \frac{1}{\sigma^2} \Re\left\{h_i^* h_j A_0[n] \Delta_{ij}[n] \dot{\gamma}_{\text{tx},i}^* \gamma_{\text{tx},j}^* \gamma_{\text{rx},i} \dot{\gamma}_{\text{rx},j} \|\mathbf{x}[n]\|^2\right\} \tag{52}
$$
$$
\Phi(\theta_{\text{tx},i}, h_{R,j}, n)
$$
$$
= \frac{1}{\sigma^2} \Re\left\{h_i^* A_0[n] \Delta_{ij}[n] \dot{\gamma}_{\text{tx},i}^* \gamma_{\text{tx},j}^* \gamma_{\text{rx},i} \gamma_{\text{rx},j}^* \|\mathbf{x}[n]\|^2\right\} \tag{53}
$$
$$
\Phi(\theta_{\text{tx},i}, h_{I,j}, n)
$$
$$
= \frac{1}{\sigma^2} \Re\left\{jh_i^* A_0[n] \Delta_{ij}[n] \dot{\gamma}_{\text{tx},i}^* \gamma_{\text{tx},j}^* \gamma_{\text{rx},i} \gamma_{\text{rx},j}^* \|\mathbf{x}[n]\|^2\right\} \tag{54}
$$
$$
\Phi(\theta_{\text{rx},i}, h_{R,j}, n)
$$
$$
= \frac{1}{\sigma^2} \Re\left\{h_i^* A_0[n] \Delta_{ij}[n] \gamma_{\text{tx},i} \gamma_{\text{tx},j}^* \dot{\gamma}_{\text{rx},i}^* \gamma_{\text{rx},j}^* \|\mathbf{x}[n]\|^2\right\} \tag{55}
$$

$$
\mathbf{J}_{(i,j)} = \begin{bmatrix}
\Phi(\tau_i, \tau_j) & \Phi(\tau_i, \theta_{\mathrm{tx},j}) & \Phi(\tau_i, \theta_{\mathrm{rx},j}) & \Phi(\tau_i, h_{R,j}) & \Phi(\tau_i, h_{I,j}) \\
\Phi(\theta_{\mathrm{tx},i}, \tau_j) & \Phi(\theta_{\mathrm{tx},i}, \theta_{\mathrm{tx},j}) & \Phi(\theta_{\mathrm{tx},i}, \theta_{\mathrm{rx},j}) & \Phi(\theta_{\mathrm{tx},i}, h_{R,j}) & \Phi(\theta_{\mathrm{tx},i}, h_{I,j}) \\
\Phi(\theta_{\mathrm{rx},i}, \tau_j) & \Phi(\theta_{\mathrm{rx},i}, \theta_{\mathrm{tx},j}) & \Phi(\theta_{\mathrm{rx},i}, \theta_{\mathrm{rx},j}) & \Phi(\theta_{\mathrm{rx},i}, h_{R,j}) & \Phi(\theta_{\mathrm{rx},i}, h_{I,j}) \\
\Phi(h_{R,i}, \tau_j) & \Phi(h_{R,i}, \theta_{\mathrm{tx},j}) & \Phi(h_{R,i}, \theta_{\mathrm{rx},j}) & \Phi(h_{R,i}, h_{R,j}) & \Phi(h_{R,i}, h_{I,j}) \\
\Phi(h_{I,i}, \tau_j) & \Phi(h_{I,i}, \theta_{\mathrm{tx},j}) & \Phi(h_{I,i}, \theta_{\mathrm{rx},j}) & \Phi(h_{I,i}, h_{R,j}) & \Phi(h_{I,i}, h_{I,j})
\end{bmatrix}
\tag{35}
$$

$\Phi(\theta_{\mathrm{rx},i}, h_{I,j}, n)$

$$
= \frac{1}{\sigma^2} \Re \left\{ jh_i^* A_0 \Delta_{ij}[n] \gamma_{\mathrm{tx},i} \gamma_{\mathrm{tx},i}^* \dot{\gamma}_{\mathrm{rx},i}^* \gamma_{\mathrm{rx},i}^* \|\mathbf{x}[n]\|^2 \right\}
\tag{56}
$$

$\Phi(h_{R,i}, h_{I,i}, n)$

$$
= \frac{1}{\sigma^2} \Re \left\{ jA_0 \Delta_{ij}[n] \gamma_{\mathrm{tx},i} \gamma_{\mathrm{tx},j}^* \gamma_{\mathrm{rx},i} \gamma_{\mathrm{rx},j}^* \|\mathbf{x}[n]\|^2 \right\},
\tag{57}
$$

and for the lower diagonal as:

$\Phi(\theta_{\mathrm{tx},i}, \tau_j, n)$

$$
= -\frac{1}{\sigma^2} \Re \left\{ jh_i^* h_j A_1[n] \Delta_{ij}[n] \dot{\gamma}_{\mathrm{tx},i}^* \gamma_{\mathrm{tx},j}^* \gamma_{\mathrm{rx},i} \gamma_{\mathrm{rx},j}^* \|\mathbf{x}[n]\|^2 \right\}
\tag{58}
$$

$\Phi(\theta_{\mathrm{rx},i}, \tau_j, n)$

$$
= -\frac{1}{\sigma^2} \Re \left\{ jh_i^* h_j A_1[n] \Delta_{ij}[n] \gamma_{\mathrm{tx},i} \gamma_{\mathrm{tx},j}^* \dot{\gamma}_{\mathrm{rx},i}^* \gamma_{\mathrm{rx},j}^* \|\mathbf{x}[n]\|^2 \right\}
\tag{59}
$$

$\Phi(h_{R,i}, \tau_j, n)$

$$
= -\frac{1}{\sigma^2} \Re \left\{ jh_j A_1[n] \Delta_{ij}[n] \gamma_{\mathrm{tx},i} \gamma_{\mathrm{tx},j}^* \gamma_{\mathrm{rx},i} \gamma_{\mathrm{rx},j}^* \|\mathbf{x}[n]\|^2 \right\}
\tag{60}
$$

$\Phi(h_{I,i}, \tau_j, n)$

$$
= -\frac{1}{\sigma^2} \Re \left\{ h_j A_1[n] \Delta_{ij}[n] \gamma_{\mathrm{tx},i} \gamma_{\mathrm{tx},j}^* \gamma_{\mathrm{rx},i} \gamma_{\mathrm{rx},j}^* \|\mathbf{x}[n]\|^2 \right\}
\tag{61}
$$

$\Phi(\theta_{\mathrm{rx},i}, \theta_{\mathrm{tx},j}, n)$

$$
= \frac{1}{\sigma^2} \Re \left\{ h_i^* h_j A_0[n] \Delta_{ij}[n] \gamma_{\mathrm{tx},i} \dot{\gamma}_{\mathrm{tx},j} \dot{\gamma}_{\mathrm{rx},i}^* \gamma_{\mathrm{rx},j}^* \|\mathbf{x}[n]\|^2 \right\}
\tag{62}
$$

$\Phi(h_{R,i}, \theta_{\mathrm{tx},j}, n)$

$$
= \frac{1}{\sigma^2} \Re \left\{ h_j A_0[n] \Delta_{ij}[n] \gamma_{\mathrm{tx},i} \dot{\gamma}_{\mathrm{tx},j} \gamma_{\mathrm{rx},i} \gamma_{\mathrm{rx},j}^* \|\mathbf{x}[n]\|^2 \right\}
\tag{63}
$$

$\Phi(h_{I,i}, \theta_{\mathrm{tx},j}, n)$

$$
= -\frac{1}{\sigma^2} \Re \left\{ jh_j A_0[n] \Delta_{ij}[n] \gamma_{\mathrm{tx},i} \dot{\gamma}_{\mathrm{tx},j} \gamma_{\mathrm{rx},i} \gamma_{\mathrm{rx},j}^* \|\mathbf{x}[n]\|^2 \right\}
\tag{64}
$$

$\Phi(h_{R,i}, \theta_{\mathrm{rx},j}, n)$

$$
= \frac{1}{\sigma^2} \Re \left\{ h_j A_0[n] \Delta_{ij}[n] \gamma_{\mathrm{tx},i} \gamma_{\mathrm{tx},j}^* \gamma_{\mathrm{rx},i} \dot{\gamma}_{\mathrm{rx},j} \|\mathbf{x}[n]\|^2 \right\}
\tag{65}
$$

$\Phi(h_{I,i}, \theta_{\mathrm{rx},j}, n)$

$$
= -\frac{1}{\sigma^2} \Re \left\{ jh_j A_0[n] \Delta_{ij}[n] \gamma_{\mathrm{tx},i} \gamma_{\mathrm{tx},j}^* \gamma_{\mathrm{rx},i} \dot{\gamma}_{\mathrm{rx},j} \|\mathbf{x}[n]\|^2 \right\}
\tag{66}
$$

$\Phi(h_{I,i}, h_{R,j}, n)$

$$
= -\frac{1}{\sigma^2} \Re \left\{ jA_0[n] \Delta_{ij}[n] \gamma_{\mathrm{tx},i} \gamma_{\mathrm{tx},j}^* \gamma_{\mathrm{rx},i} \gamma_{\mathrm{rx},j}^* \|\mathbf{x}[n]\|^2 \right\}.
\tag{67}
$$

REFERENCES

[1] Z. Pi and F. Khan, "An introduction to millimeter-wave mobile broadband systems," *IEEE Commun. Mag.*, vol. 49, no. 6, pp. 101–107, Jun. 2011.

[2] T. S. Rappaport, S. Sun, R. Mayzus, H. Zhao, Y. Azar, K. Wang, George N. Wong, J. K. Schulz, M. Samimi, and F. Gutierrez, "Millimeter wave mobile communications for 5G cellular: It will work," *IEEE Access*, vol. 1, pp. 335–349, 2013.

[3] A. L. Swindlehurst, E. Ayanoglu, P. Heydari, and F. Capolino, "Millimeter-wave massive MIMO: The next wireless revolution," *IEEE Commun. Mag.*, vol. 52, no. 9, pp. 56–62, Sep. 2014.

[4] M. Giordani, M. Mezzavilla, and M. Zorzi, "Initial access in 5G mmWave cellular networks," *IEEE Commun. Mag.*, vol. 54, no. 11, pp. 40–47, Nov. 2016.

[5] M. Shafi, A. F. Molisch, P. J. Smith, T. Haustein, P. Zhu, P. De Silva, F. Tufvesson, A. Benjebbour, and G. Wunder, "5G: A tutorial overview of standards, trials, challenges, deployment, and practice," *IEEE J. Sel. Areas Commun.*, vol. 35, no. 6, pp. 1201–1221, Jun. 2017.

[6] K. Venugopal and R. W. Heath, Jr., "Millimeter wave networked wearables in dense indoor environments," *IEEE Access*, vol. 4, pp. 1205–1221, 2016.

[7] J. Choi, V. Va, and N. Gonzalez-Prelcic, R. Daniels, C. R. Bhat, and R. W. Heach, Jr., "Millimeter-wave vehicular communication to support massive automotive sensing," *IEEE Commun. Mag.*, vol. 54, no. 12, pp. 160–167, Dec. 2016.

[8] J. Wang, Z. Lan, C.-W. Pyo, T. Baykas, C.-S. Sum, M. A. Rahman, R. Funada, F. Kojima, I. Lakkis, H. Harada, and S. Kato, "Beam codebook based beamforming protocol for multi-Gbps millimeter-wave WPAN systems," *IEEE J. Sel. Areas Commun.*, vol. 27, no. 8, pp. 1390–1399, Oct. 2009.

[9] S. Hur, T. Kim, D. J. Love, J. V. Krogmeier, T. A. Thomas, and A. Ghosh, "Millimeter wave beamforming for wireless backhaul and access in small cell networks," *IEEE Trans. Commun.*, vol. 61, no. 10, pp. 4391–4403, Oct. 2013.

[10] Y. Tsang, A. S. Y. Poon, and S. Addepalli, "Coding the beams: Improving Beamforming training in mm Wave communication system," in *Proc. IEEE Global Commun. Conf.*, Dec. 2011, pp. 1–6.

[11] R. J. Lopes and J. M. Brazio, "A geometry-based statistical model for fast fading in millimeterwave communications," in *Proc. IEEE 45th Veh. Technol. Conf. Countdown Wireless 21st Century*, vol. 1, Jul. 1995, pp. 459–463.

[12] H. Deng and A. Sayeed, "Mm-wave MIMO channel modeling and user localization using sparse beamspace signatures," in *Proc. 15th Int. Workshop Signal Process. Adv. Wireless Commun. (SPAWC)*, Jun. 2014, pp. 130–134.

[13] Q. Li, G. Wu, and T. S. Rappaport, "Channel model for millimeter-wave communications based on geometry statistics," in *Proc. IEEE Global Commun. Conf. Workshops*, Dec. 2014, pp. 427–432.

[14] A. Alkhateeb, O. El Ayach, G. Leus, and R. W. Heath, Jr., "Channel estimation and hybrid precoding for millimeter wave cellular systems," *IEEE J. Sel. Topics Signal Process.*, vol. 8, no. 5, pp. 831–846, Oct. 2014.

[15] M. Steinbauer, A. F. Molisch, and E. Bonek, "The double-directional radio channel," *IEEE Antennas Propag. Mag.*, vol. 43, no. 4, pp. 51–63, Aug. 2001.

[16] Z. Abu-Shaban, X. Zhou, T. Abhayapala, G. Seco-Granados, and H. Wymeersch, "Error bounds for uplink and Downlink 3D localization in 5G millimeter wave systems," *IEEE Trans. Wireless Commun.*, vol. 17, no. 8, pp. 4939–4954, Aug. 2018.

[17] A. Shahmansoori, G. E. Garcia, G. Destino, G. Seco-Granados, and H. Wymeersch, "Position and orientation estimation through millimeter-wave MIMO in 5G systems," *IEEE Trans. Wireless Commun.*, vol. 17, no. 3, pp. 1822–1835, Mar. 2017.

[18] J. Bae, S. H. Lim, J. H. Yoo, and J. W. Choi, "New beam tracking technique for millimeter wave-band communications," 2017, *arXiv:1702.00276*. [Online]. Available: https://arxiv.org/abs/1702.00276

[19] K. Gao, M. Cai, D. Nie, B. Hochwald, J. N. Laneman, H. Huang, and K. Liu, "Beampattern-based tracking for millimeter wave communication systems," in *Proc. IEEE Global Commun. Conf.*, Dec. 2016, pp. 1–6.

[20] R. Di Taranto, S. Muppirisetty, R. Raulefs, D. Slock, T. Svensson, and H. Wymeersch, "Location-aware communications for 5G networks: How location information can improve scalability, latency, and robustness of 5G," *IEEE Signal Process. Mag.*, vol. 31, no. 6, pp. 102–112, Nov. 2014.

[21] C. N. Barati, S. A. Hosseini, M. Mezzavilla, T. Korakis, S. S. Panwar, S. Rangan, and M. Zorzi, "Initial access in millimeter wave cellular systems," *IEEE Trans. Wireless Commun.*, vol. 15, no. 12, pp. 7926–7940, Dec. 2016.

[22] V. Desai, L. Krzymien, P. Sartori, W. Xiao, A. Soong, and A. Alkhateeb, "Initial beamforming for mm wave communications," in *Proc. 48th Asilomar Conf. Signals, Syst. Comput.*, Nov. 2014, pp. 1926–1930.

[23] H.-H. Lee and Y.-C. Ko, "Low Complexity Codebook-based beamforming for MIMO-OFDM systems in millimeter-wave WPAN," *IEEE Trans. Wireless Commun.*, vol. 10, no. 11, pp. 3607–3612, Nov. 2011.

[24] Z. Xiao, T. He, P. Xia, and X.-G. Xia, "Hierarchical codebook design for beamforming training in millimeter-wave communication," *IEEE Trans. Wireless Commun.*, vol. 15, no. 5, pp. 3380–3392, May 2016.

[25] J. Singh and S. Ramakrishna, "On the feasibility of codebook-based beamforming in millimeter wave systems with multiple antenna arrays," *IEEE Trans. Wireless Commun.*, vol. 14, no. 5, pp. 2670–2683, May 2015.

[26] M. Kokshoorn, H. Chen, P. Wang, Y. Li, and B. Vucetic, "Millimeter wave MIMO channel estimation using overlapped beam patterns and rate adaptation," *IEEE Trans. Signal Process.*, vol. 65, no. 3, pp. 601–616, Feb. 2017.

[27] J. Kim and A. F. Molisch, "Fast millimeter-wave beam training with receive beamforming," *J. Commun. Netw.*, vol. 16, no. 5, pp. 512–522, Oct. 2014.

[28] S. Sur, X. Zhang, P. Ramanathan, and R. Chandra, "BeamSpy: Enabling robust 60 GHz links under blockage," in *Proc. 13th USENIX Symp. Netw. Syst. Design Implement. (NSDI)*, 2016, pp. 193–206.

[29] A. Zhou, X. Zhang, and H. Ma, "Beam-forecast: Facilitating mobile 60 GHz networks via model-driven beam steering," in *Proc. IEEE INFOCOM IEEE Conf. Comput. Commun.*, May 2017, pp. 1–9.

[30] D. Zhang, H. Chen, M. Shirvanimoghaddam, Y. Li, and B. Vucetic, "Training beam sequence optimization for millimeter wave MIMO tracking systems," in *Proc. IEEE Int. Conf. Commun. (ICC)*, May 2018, pp. 1–6.

[31] M. E. Rasekh, Z. Marzi, Y. Zhu, U. Madhow, and H. Zheng, "Noncoherent mm wave path tracking," in *Proc. 18th Int. Workshop Mobile Comput. Syst. Appl.*, Feb. 2017, pp. 13–18.

[32] H. S. Ghadikolaei, H. Ghauch, and C. Fischione, "Learning-based tracking of aoas and aods in mm wave networks," in *Proc. 2nd ACM Workshop Millim. Wave Netw. Sens. Syst.*, Oct. 2018, pp. 45–50.

[33] N. Garcia, H. Wymeersch, E. G. Ström, and D. Slock, "Location-aided mm-wave channel estimation for vehicular communication," in *Proc. IEEE Int. Workshop Signal Process. Adv. Wireless Commun.*, Jul. 2016, pp. 1–5.

[34] V. Va, X. Zhang, and R. W. Heath, Jr., "Beam switching for millimeter wave communication to support high speed trains," in *Proc. IEEE 82nd Veh. Technol. Conf. (VTC Fall)*, Sep. 2015, pp. 1–5.

[35] J. C. Aviles and A. Kouki, "Position-aided mm-wave beam training under NLOS conditions," *IEEE Access*, vol. 4, pp. 8703–8714, 2016.

[36] G. C. Alexandropoulos, "Position aided beam alignment for millimeter wave backhaul systems with large phased arrays," 2017, *arXiv:1701.03291*. [Online]. Available: https://arxiv.org/abs/1701.03291

[37] G. E. Garcia, G. Seco-Granados, E. Karipidis, and H. Wymeersch, "Transmitter beam selection in millimeter-wave MIMO with in-band position-aiding," 2017, *arXiv:1705.05668*. [Online]. Available: https://arxiv.org/abs/1705.05668

[38] A. Alkhateeb and R. W. Heath, Jr., "Frequency selective hybrid precoding for limited feedback millimeter wave systems," *IEEE Trans. Commun.*, vol. 64, no. 5, pp. 1801–1818, May 2016.

[39] N. Celik, W. Kim, M. F. Demirkol, M. F. Iskander, and R. Emrick, "Implementation and experimental verification of hybrid smart-antenna beamforming algorithm," *IEEE Antennas Wireless Propag. Lett.*, vol. 5, no. 1, pp. 280–283, Dec. 2006.

[40] R. W. Heath, Jr., N. González-Prelcic, S. Rangan, W. Roh, and A. M. Sayeed, "An overview of signal processing techniques for millimeter wave MIMO systems," *IEEE J. Sel. Topics Signal Process.*, vol. 10, no. 3, pp. 436–453, Apr. 2016.

[41] *IEEE Standard for High Data Rate Wireless Multi-Media Networks*, Standard IEEE Std 802.15.3-2016, 2016.

[42] S. M. Kay, *Fundamentals Statistical Signal Processing: Estimation Theory*. New York, NY, USA: Prentice-Hall, 2010.

[43] H. Van Trees, *Detection, Estimation, Modulation Theory*. Hoboken, NJ, USA: Wiley, 2001.

[44] M. Wax, T.-J. Shan, and T. Kailath, "Location and the spectral density estimation of multiple sources," DTIC, Fort Belvoir, VA, USA, Tech. Rep. AFOSR-TR-83-0323, 1982.

[45] M. Wax and T. Kailath, "Optimum localization of multiple sources by passive arrays," *IEEE Trans. Acoust., Speech, Signal Process.*, vol. ASSP-31, no. 5, pp. 1210–1217, Oct. 1983.

[46] M. Wax and T. Kailath, "Decentralized processing in sensor arrays," *IEEE Trans. Acoust., Speech, Signal Process.*, vol. ASSP-33, no. 5, pp. 1123–1129, Oct. 1985.

[47] A. J. Weiss, "Direct position determination of narrowband radio frequency transmitters," *IEEE Signal Process. Lett.*, vol. 11, no. 5, pp. 513–516, May 2004.

[48] X. Song, S. Haghighatshoar, and G. Caire, "A scalable and statistically robust beam alignment technique for mm-wave systems," 2017, *arXiv:1708.09433*. [Online]. Available: https://arxiv.org/abs/1708.09433

[49] D. E. Berraki, S. M. Armour, and A. Nix, "Application of compressive sensing in sparse spatial channel recovery for beamforming in mm Wave outdoor systems," in *Proc. IEEE Wireless Commun. Netw. Conf. (WCNC)*, Apr. 2014, pp. 887–892.

[50] A. Alkhateeb, G. Leus, and R. W. Heath, Jr., "Compressed sensing based multi-user millimeter wave systems: How many measurements are needed," in *Proc. IEEE Int. Conf. Acoust., Speech Signal Process. (ICASSP)*, Apr. 2015, pp. 2909–2913.

[51] J. Choi, "Beam selection in mm-wave multiuser MIMO systems using compressive sensing," *IEEE Trans. Commun.*, vol. 63, no. 8, pp. 2936–2947, Aug. 2015.

[52] K. Venugopal, A. Alkhateeb, N. G. Prelcic, and R. W. Heath, "Channel estimation for hybrid architecture based wideband millimeter wave systems," *IEEE J. Sel. Areas Commun.*, vol. 35, no. 9, pp. 1996–2009, Sep. 2017.

[53] J. Talvitie, M. Valkama, G. Destino, and H. Wymeersch, "Novel algorithms for high-accuracy joint position and orientation estimation in 5G mm wave systems," in *Proc. IEEE Globecom Workshops (GC Wkshps)*, Dec. 2017, pp. 1–7.

[54] G. Destino and H. Wymeersch, "On the trade-off between positioning and data rate for mm-wave communication," in *Proc. IEEE Int. Commun. Conf. Workshops (ICC Workshops)*, May 2017, pp. 797–802.

[55] R. J. Muirhead, *Aspects Multivariate Statistical Theory*. Hoboken, NJ, USA: Wiley, 2005.

GABRIEL E. GARCIA received the B.Sc. degree in electronics and communication engineering from the Instituto Tecnológico y de Estudios Superiores de Monterrey, Querétaro, Mexico, in 2007, and the M.Sc. degree in communication, the Licentiate degree, and the Ph.D. degree in electrical engineering from Chalmers University of Technology, Gothenburg, Sweden, in 2010, 2013, and 2019, respectively. His research interests include cooperative networks, robust radio frequency localization and navigation, UWB, mm-wave, wireless sensor networks, GNSS, statistical inference, and sensor fusion.

NIL GARCIA (S'14–M'16) received the Telecommunications Engineer degree from the Polytechnic University of Catalonia, Barcelona, Spain, in 2008, and the Ph.D. degrees in electrical engineering from the New Jersey Institute of Technology, Newark, NJ, USA, and the National Polytechnic Institute of Toulouse, Toulouse, France, in 2015. In 2009, he was an Engineer with the Centre National d'Etudes Spatiales. He had internships in CNES and NASA, in 2008 and 2009. He is currently a Postdoctoral Researcher of communication systems with the Department of Electrical Engineering, Chalmers University of Technology, Gothenburg, Sweden. His research interests include the areas of localization, intelligent transportation systems, and 5G.

GONZALO SECO-GRANADOS (S'97–M'02–SM'08) received the Ph.D. degree in telecommunications engineering from the Universitat Politècnica de Catalunya, Spain, in 2000, and the M.B.A. degree from the IESE Business School, Spain, in 2002. From 2002 to 2005, he was a member of the European Space Agency, where he was involved in the design of the Galileo system. In 2015, he was a Fulbright Visiting Professor with the University of California at Irvine, Irvine, CA, USA. Since 2006, he has been with the Department of Telecommunications, Universitat Autònoma de Barcelona, where he has been the Vice Dean of the Engineering School, since 2011, and is currently a Professor. His research interests include satellite and terrestrial localization systems. Since 2018, he has been serving as a member for the Sensor Array and Multichannel Technical Committee of the IEEE Signal Processing Society. He was a recipient of the 2013 ICREA Academia Award.

HENK WYMEERSCH (S'01–M'05) received the Ph.D. degree in electrical engineering/applied sciences from Ghent University, Belgium, in 2005. He was a Postdoctoral Researcher with the Laboratory for Information and Decision Systems, Massachusetts Institute of Technology, from 2005 to 2009. He is currently a Professor of communication systems with the Department of Electrical Engineering, Chalmers University of Technology, Sweden. His current research interests include cooperative systems and intelligent transportation. He has served as an Associate Editor for the IEEE Communications Letters, from 2009 to 2013, and the IEEE Transactions on Communications, from 2016 to 2018. He has been serving as an Associate Editor for the IEEE Transactions on Wireless Communications, since 2013.

• • •

ELEFTHERIOS KARIPIDIS (S'05–M'09) received the Diploma degree in electrical and computer engineering from the Aristotle University of Thessaloniki, Greece, in 2001, the M.Sc. degree in communications engineering from the Technical University of Munich, Germany, in 2003, and the Ph.D. degree in electronic and computer engineering from the Technical University of Crete, Chania, Greece, in 2008. From 2008 to 2013, he was with the Communication Systems Division, Department of Electrical Engineering, Linköping University, Sweden. Since 2013, he has been with Ericsson Research, Stockholm, Sweden, where he is currently a Senior Researcher. He is involved in the standardization of 5G New Radio in 3GPP, since Release 15, with a focus on multiple-input multiple-output and reference signals. From 2016 to 2018, he was a member of the Signal Processing for Communications and Networking Technical Committee of the IEEE Signal Processing Society.